



Available online at www.sciencedirect.com

ScienceDirect

Soils and Foundations 62 (2022) 101235



www.elsevier.com/locate/sandf

Technical Paper

Coupled solute transport through a polymer-enhanced bentonite

Shan Tong ^{a,1}, Kristin M. Sample-Lord ^{b,*}

^a MOE Key Laboratory of Soft Soils and Geoenvironmental Engineering, College of Civil Engineering and Architecture, Zhejiang University, Hangzhou 310058, China

^b Department of Civil and Environmental Engineering, 800 Lancaster Avenue, Villanova University, Villanova, PA 19085, USA

Received 20 February 2022; received in revised form 12 September 2022; accepted 25 September 2022 Available online 7 October 2022

Abstract

Polymer-enhanced bentonites for geoenvironmental containment barriers, such as bentonite-polyacrylic-acid composite (BPC), generally have low hydraulic conductivity (e.g., $k < 10^{-10}$ m/s) even when exposed to aggressive waste solutions. However, understanding of diffusion and membrane behavior properties of enhanced bentonites and associated impacts on coupled contaminant transport through the barrier remains limited. In this study, hydraulic conductivity (k), effective diffusion coefficients (D^*), and membrane efficiencies (ω) were measured for BPC with 3.2 % polymer content (by mass; referred to as BPC-3.2). Tests were performed with potassium chloride (KCl) solutions ranging from dilute (2.5 mM) to aggressive (400 mM) concentrations. As concentration increased, D^* increased by a factor of three, ω decreased by two orders of magnitude, and k remained relatively low (1.2 × 10⁻¹¹ to 2.9 × 10⁻¹¹ m/s). The experimental results were paired with an existing coupled solute transport model to evaluate the significance of membrane behavior and diffusion on predicted total solute flux through a geosynthetic clay liner (GCL) and a GCL overlying an attenuation layer. The predicted mass flux was diffusion dominated, with the diffusive flux greater than the advective flux by one to two orders of magnitude. Membrane behavior reduced predicted total solute flux through the GCL by 5.8 to 61 %. The results demonstrate the role of coupled solute transport in the long-term performance of bentonite barriers, and advance understanding of contaminant transport in BPC.

© 2022 Production and hosting by Elsevier B.V. on behalf of The Japanese Geotechnical Society. This is an open access article under the CC BY-NC-ND license (http://creativecommons.org/licenses/by-nc-nd/4.0/).

Keywords: Bentonite polymer composite; Coupled solute transport; Geosynthetic clay liner; Diffusion; Membrane behavior

1. Introduction

Sodium bentonite (NaB) is a common barrier material for waste containment applications due to the high osmotic swelling and low hydraulic conductivity (k) of NaB to water (e.g., 5×10^{-11} m/s; Rowe, 2012) which limits advective flux of contaminants into the environment. However, NaB may undergo adverse chemical interactions when

Peer review under responsibility of The Japanese Geotechnical Society.

exposed to liquids with multivalent cationic species, high ionic strength, and/or extreme pH (2 > pH > 12). The resulting deterioration in hydraulic performance of the NaB barrier (i.e., increase in k), commonly referred to as chemical incompatibility, has been widely investigated throughout the literature (e.g., Kolstad et al., 2004; Benson and Meer, 2009; Gates and Bouazza, 2010; Hornsey et al., 2010).

To address chemical incompatibility issues associated with NaB, there has been increased focus over the last three decades on development of enhanced bentonites (EBs) for improved hydraulic resilience (e.g., see review in Scalia et al., 2018). The most common type of EB, bentonite-polymer composite (BPC), has been shown to maintain low k (e.g., $k < 10^{-10}$ m/s), even upon exposure to solutions

^{*} Corresponding author.

E-mail addresses: stong@zju.edu.cn (S. Tong), kristin.sample-lord@-villanova.edu (K.M. Sample-Lord).

¹ Formerly, Ph.D. student, Department of Civil and Environmental Engineering, 800 Lancaster Avenue, Villanova University, Villanova, PA 19085, USA.

with high ionic strength and/or multivalent cation concentrations (although there generally is a limit on ionic strength beyond which higher k may still occur; e.g., Scalia et al., 2014; Li et al., 2021b). Since diffusion is the dominant mechanism by which contaminants transport through the barrier when $k < 10^{-10}$ m/s, numerous experimental studies have investigated solute diffusion coefficients for NaB (Shackelford, 2014). However, very little is known about solute diffusion through BPC barriers (Tong et al., 2021). In addition, BPC has been shown to exhibit significant membrane behavior (e.g., Bohnhoff and Shackelford, 2013), which reduces total solute flux through the barrier. However, experimental data in the literature for membrane behavior of BPC and other polymeramended bentonites has also remained limited.

To predict long-term coupled contaminant transport through a bentonite barrier, values of k, effective diffusion coefficients (D^*) , and membrane efficiencies (ω) of the bentonite as a function of the solution/leachate properties must be known (Mitchell, 1993). Therefore, in this study, values of k, D^* , and ω were measured for a BPC with 3.2 % polymer content (hereafter referred to as BPC-3.2) for KCl solutions with concentrations ranging from dilute (2.5 mM) to aggressive (400 mM). A multi-stage throughdiffusion and membrane behavior test was performed to simultaneously measure D^* and ω over the range of concentrations. Values of k were measured via multi-stage hydraulic conductivity testing for the same concentration range. The results of the tests (i.e., values of ω , D^* , and kas a function of concentration) were combined with an existing coupled solute transport model to compare the predicted steady-state coupled solute flux across the barrier for different materials and conditions. The results of the study support data-informed comparisons of expected long-term performance for NaB and BPC barriers.

2. Background

2.1. Hydraulic conductivity and diffusion coefficients of bentonite polymer composites

Many studies have reported enhanced swelling and hydraulic properties of BPC geosynthetic clay liners (GCLs) for aggressive solutions, relative to NaB GCLs, with k typically ranging from 10^{-12} m/s to 10^{-10} m/s (e.g., Scalia et al., 2014; Tian and Benson, 2015). The low k of most BPC products has primarily been attributed to the clogging of polymer hydrogels between the bentonite granules that result in less pore space and more tortuous flow pathways (e.g., Tian et al., 2016b, 2019). At low k ($\leq 10^{-10}$ m/s), advection of contaminants is restricted such that diffusion becomes a significant to dominant transport mechanism through the barrier (Rowe et al., 1988; Lake and Rowe, 2000). Although there has been extensive study since the 1960s on the importance of diffusion for NaB barriers (e.g., Dutt and Low, 1962; Kemper and van Schaik,

1966), BPC research typically does not include corresponding measurement of diffusion properties.

Typically, solute diffusion through the clay barrier can be expressed by the Fickian process, in which the diffusion coefficient of the solute can be expressed as (Malusis and Shackelford, 2002b):

$$D^* = D_0 \tau_a = D_0 \tau_m \tau_r = D_{se} \tau_r \tag{1}$$

where n is total porosity [-], D^* is the effective diffusion coefficient $[L^2T^{-1}]$, D_o is the aqueous-phase (free-solution) diffusion coefficient of the solute $[L^2T^{-1}]$, D_{se} is the effective salt-diffusion coefficient $[L^2T^{-1}]$, τ_a is the apparent tortuosity factor [-], τ_m is the matrix tortuosity factor due to the geometry of the interconnected pores, and τ_r is the restrictive tortuosity factor which accounts for other factors hindering diffusion of solutes (e.g., semipermeable membrane behavior).

For NaB GCLs, values of D^* for chloride typically range from 10^{-11} to 10^{-9} m²/s when testing with simple salt solutions (NaCl, KCl, CaCl₂), and generally increase with increasing ionic strength and cation valence of the solution (e.g., Malusis and Shackelford, 2002b; Di Emidio et al., 2015; Dominijanni et al., 2018). The limited number of laboratory studies that have been performed to evaluate D^* for BPC have generally indicated D^* values for BPC are either similar to or lower than those for NaB (i.e., D^* for Cl⁻ for BPC ranging from 10^{-12} to 10^{-9} m²/s; Bohnhoff and Shackelford, 2015; Tong et al., 2021).

2.2. Membrane behavior and coupled transport in bentonite barriers

In clays, electrostatic repulsion associated with the diffuse double layer causes the phenomenon known as semipermeable membrane behavior (also known as membrane action or anion exclusion; Rowe et al., 2004). In particular, bentonite has been shown to exhibit significant membrane behavior, resulting in selective restriction of aqueous miscible chemical species from entering the pores (Shackelford, 2013). Membrane behavior exists when the electrostatic fields associated with two adjacent clay minerals overlap and result in repulsion of charged solutes. Membrane behavior is quantified by the membrane efficiency coefficient, or reflection coefficient, ω (0 < ω < 1), with zero indicating no solute restriction (i.e., no membrane behavior) and unity indicating complete chemical restriction (i.e., perfect semi-permeable membrane behavior) (Mitchell, 1993). Typically, ω is dependent on the type and amount of clay minerals and the pore sizes in the soil matrix, and the type and concentrations of ionic species in the pore water (Kemper and Rollins, 1966). Significant membrane behavior has been experimentally proven to exist in NaB and NaB-GCLs (e.g., Malusis and Shackelford, 2002a; Kang and Shackelford, 2011; Meier et al., 2014; Shackelford et al., 2016; Dominijanni et al., 2018; Sample-Lord and Shackelford, 2018), as well as in BPC-

GCLs (Bohnhoff and Shackelford, 2013, 2015; Bohnhoff et al., 2014) and other EBs (Mazzieri et al., 2010; Di Emidio et al., 2015; Malusis and Daniyarov, 2016; Fu et al., 2021).

Membrane behavior can improve the performance of a containment barrier by partially restricting charged solutes from passing through the pore space, resulting in reduced total contaminant flux across the barrier into the environment. In a clay exhibiting membrane behavior, the transport of solutes through the barrier is reduced via three mechanisms: (1) hyperfiltration, (2) restricted solute diffusion, and (3) chemico-osmotic counter advection (Malusis et al., 2021). The advective flux of contaminants due to the hydraulic gradient across the barrier is reduced by hyperfiltration (filtering of the flow due to membrane behavior). The diffusive flux due to the chemical gradient across the barrier is reduced by anion exclusion (resulting in a lower D^* value). Finally, the existence of membrane behavior may also result in chemico-osmotic counterflow, whereby liquid flows from the lower solute concentration side (higher water activity) to the higher solute concentration side of the barrier (Shackelford, 2013).

Manassero and Dominijanni (2003) developed a theoretical framework for coupled fluxes in saturated incompressible porous medium, combining phenomenological expressions including mass flow equations derived from the dissipation function for the coupled flow process using the second postulate of irreversible thermodynamics (Katchalsky and Curran, 1965), mass balance equations for the solute and the solvent, and the continuity equation for solvent flux. Under this framework, the following differential equations represent the solute concentration and solution pressure as a function of time and distance:

$$\omega RT \frac{\partial^2 C_j}{\partial x^2} - \frac{\partial^2 P}{\partial x^2} = 0 \tag{3}$$

$$R_{d} \frac{\partial C_{j}}{\partial t} = (1 - \omega) \left\{ \left[(\tau D_{o}) - \frac{\omega kRT}{\gamma n} c_{j} \right] \frac{\partial^{2} C_{j}}{\partial x^{2}} - \frac{k}{\gamma n} \frac{\partial}{\partial t} \left(-\frac{\partial P}{\partial x} c_{j} \right) - \frac{\omega kRT}{\gamma n} \left(-\frac{\partial C_{j}}{\partial x} \right)^{2} \right\}$$
(4)

where C_j is the concentration of species j, x is the direction of transport, P is hydraulic pressure, R_d is the retardation factor, R is the universal gas constant, T is absolute temperature, k is hydraulic conductivity, and γ is unit weight of the solution.

Based on the theoretical framework, the total solute mass flux occurring through a horizontal clay layer of thickness L from the upper boundary (high concentration side) to the lower boundary (lower concentration side) can be determined for steady-state solute flow conditions (i.e., $\frac{\partial C_i}{\partial t} = 0$) and the following boundary conditions:

$$P(x=0) = P_t = h_t \gamma = \text{constant}$$
 (5)

$$P(x = L) = P_b = h_b \gamma = \text{constant}$$
 (6)

$$C_i(x=0) = C_t = \text{constant} \tag{7}$$

$$C_i(x=L) = C_b = \text{constant}$$
 (8)

That is (Manassero and Dominijanni, 2003; Malusis et al., 2012, 2020),

$$J'_{j} = (1 - \omega)\left(-k\frac{h_{b} - h_{t}}{L}\right)C_{j} + (1 - \omega)\left(\omega\frac{k}{\gamma_{w}}\frac{v}{v_{j}}RT\right)$$

$$\times \frac{C_{b} - C_{t}}{L}C_{j} - nD^{*}\frac{C_{b} - C_{t}}{L}$$
(9)

where J_j is the total solute mass flux [ML⁻²T⁻¹], v is number of ions per molecule of salt (e.g., v = 2 for KCl), v_j is number of ions of species j per molecule of salt (e.g., v_j = 1 for Cl⁻¹ in KCl), and subscripts "b" and "t" denote the bottom and top boundaries, respectively. It should be noted that Equation (9) represents an approximate (rather than exact) solution in which all of the transport components have been linearized separately.

In Equation (9), the first term represents the advective flux (J_a) , accounting for hyperfiltration effects due to membrane behavior, the second term represents the osmotic flux (J_π) occurring in the counter-direction due to membrane behavior, and the last term represents the diffusive flux (J_d) , accounting for reduced diffusion due to ion restriction. In low-k barriers where diffusion is the dominant transport process $(J_d > J_a)$, restricted diffusion is the most significant mechanism by which membrane behavior reduces solute flux and improves containment.

When membrane behavior does not exist (i.e., $\omega = 0$), Equation (9) reduces to:

$$J_j = \left(-k\frac{h_b - h_t}{L}\right)C_j - nD^*\frac{C_b - C_t}{L} \tag{10}$$

where J_j is the total solute mass flux through the clay without membrane behavior.

In clays exhibiting membrane behavior, the restrictive tortuosity can be considered as the complement number of the membrane efficiency, i.e., $\tau_r = 1-\omega$ (Dominijanni et al., 2013), such that D_{se} can also be expressed as:

$$D_{se} = \frac{D^*}{1 - \omega} \tag{11}$$

As seen in Equation (9), to predict the total solute mass flux across a bentonite barrier exhibiting membrane behavior, values of ω , k, and D^* must be known for the specific bentonite type and relevant environmental conditions (solution chemistry, porosity, temperature, etc.). Although laboratory studies have demonstrated the existence of membrane behavior in BPC, the persistence of membrane behavior at high concentrations (e.g., > 50 mM KCl) and low polymer content (e.g., \le 5% by mass) has not been evaluated. Further, very few studies have measured all three parameters (ω , k, and D^*) for the same BPC material and salt solution.

3. Materials and methods

3.1. Bentonite and test solutions

The BPC was a mixture of a NaB and a sodiumpolyacrylate-amended bentonite, resulting in a total polymer content of 3.2 % (hereafter referred to as BPC-3.2). The polymer content of current commercial BPC products generally ranges from 0.5% - 12% (e.g., Tian et al., 2016a; Chen et al., 2019; Li et al., 2021a,b; Wireko et al., 2022), with more recent emphasis on the lower side of the range (e.g., 4 %). The BPC in this study was prepared by dryblending of: (1) GCL-grade NaB that has been used in the production of Bentomat® (Colloid Environmental Technologies Company, CETCO, Hoffman Estates, IL); and (2) a sodium polyacrylate (PAAS)-bentonite composite that had been manufactured by in-situ polymerization as described by Muzny et al. (1996) and Scalia et al. (2014) (denoted as "BPN" or "BPC" in the literature), at a ratio of 9:1 (by mass). Physical and chemical properties of the NaB and BPC are summarized in Table 1. Details of the polymer properties were proprietary. The polymer content (X_P) of 3.2 % (by dry mass) was determined through the loss on ignition (LOI) method in accordance with ASTM D7348 (ASTM 2013) and Gustitus et al. (2021).

KCl solutions used in this study was prepared with Type II deionized water and certified A.C.S level KCl (Fisher Scientific, Fair Lawn, NJ). The target concentrations ranged from 2.5 to 400 mM, to cover a spectrum from weak

to aggressive solutions that would be comparable with existing literature. The electrical conductivity (EC), pH, temperature (T) and Cl⁻ concentration ($C_{\text{Cl-}}$) of testing solutions and collected water samples were measured with an OrionTM VERSA STAR pH/Conductivity meter with probes for: EC (Orion 013005MD Conductivity Cell), pH (Orion 8157BNUMD ROSS Ultra pH/ATC Triode), and $C_{\text{Cl-}}$ (Orion 9617BNWP Ionplus Sure-Flow Solid State Combination Probe) (Thermo Fisher Scientific, Hanover Park, IL). The Cl⁻ concentrations of randomly selected solutions were also confirmed with EasyChem, a discrete nutrient analyzer with photospectrometer (Chinchilla Scientific[®] Simplicity, Chinchilla Scientific LLC, Oak Brook, IL).

3.2. Hydraulic conductivity and swell index tests

A multi-stage hydraulic conductivity (k) test was conducted in accordance with ASTM D5084 (ASTM 2010) and ASTM D6766 (ASTM 2018), using the falling-headwa ter/raising-tailwater method and a flexible-wall cell connected to bladder accumulators. The k-test specimen had a dry mass per unit area of 4.8 kg/m² and an initial n of 0.78. The specimen was saturated and permeated with DIW prior to permeation with salt solution. During permeation, the effective stress and hydraulic gradient were maintained at 34.5 kPa (5 psi) and 300, respectively. The hydraulic and chemical equilibrium termination criteria specified in ASTM D5084 and D6766 were checked prior

Table 1
Physical and chemical properties of the sodium bentonite (NaB) and sodium-polyacrylate-amended bentonite (BPC) used to create the BPC-3.2 mixture.

Property	Standard	Average for NaB [No. Trials]	Average for BPC [No. Trials] ^b
Specific Gravity	ASTM D854	2.71 [10] ^a	2.67
Soil Classification	ASTM D2487	CH [3] ^a	CH [3]
Clay (%)	ASTM D422	90 [3] ^a	96 [3]
Atterberg Limits (%):	ASTM D4318		
Liquid Limit, LL		420 [3]	255 [2]
Plasticity Index, PI		381 [4] ^a	NA ^d
Principal Minerals (%):		(100)	(100) ^e
Montmorillonite		91	73–77
Quartz		2	15–17
Plagioclase Feldspar	Ċ	3	4–5
Calcite		1	NA
Ferroan Dolomite		Trace	NA
Gypsum		1	NA
Illite / Mica		2	2
Cation exchange capacity, CEC (meq/100 g)	ASTM D7503	78.3 [6] ^a	142.6
Bound Cations (molar ratio):			
Calcium (Ca ²⁺)		36	6
Magnesium (Mg ²⁺)		15	2
Sodium (Na ⁺)		47	90
Potassium (K ⁺)		2	2

^a Based on Sample-Lord and Shackelford (2018).

b Based on Bohnhoff and Shackelford (2013) and Scalia et al. (2014).

^c Based on X-ray diffraction (XRD) analyses performed by Mineralogy, Inc., Tulsa, OK.

^d The plastic limit of the BPC could not be determined due to the "silly putty" behavior caused by the polymer additive (Bohnhoff and Shackelford 2013).

^e The principal minerals are based on Scalia et al. (2014).

to advancing to the next salt solution concentration stage. The EC of the effluent was used to monitor chemical equilibrium (i.e., $0.9 \le EC_{\text{(influent)}}/EC_{\text{(effluent)}} \le 1.1$). At least 2 pore volumes of flow (PVF) were achieved for all permeation stages. Due to the long testing durations (78 to 108 days for each salt concentration stage; Table 2), an intermediate concentration stage between 10 and 100 mM KCl could not be included.

To support interpretation of the other test results and comparisons with literature, the swell indices (*SI*) of NaB, BPC-3.2 and BPC were measured for DIW and KCl solutions with concentrations of 10, 20, 50, 100, 200, and 400 mM, in general accordance with ASTM D5890 (ASTM 2019).

3.3. Multi-stage through-diffusion and membrane behavior tests

Values of D^* and ω were measured for BPC-3.2 over a range of KCl concentrations via a multi-stage through-diffusion and membrane behavior test. The closed-system apparatus used for testing was identical to equipment previously described by Malusis et al. (2001) and Bohnhoff and Shackelford (2015). A schematic of the apparatus is shown in Fig. 1. The dry mass per unit area of the specimen was identical to that in the hydraulic conductivity test (4.8 kg/m²). The specimen thickness and diameter were 18 mm and 71 mm, respectively, and the n was 0.90. The n value was selected to allow for comparison with the membrane behavior literature (e.g., Bohnhoff and Shackelford (2015) for BPC at n = 0.80–0.92). The specimen was permeated and saturated with DIW prior to initiating the through-diffusion/membrane behavior testing sequence.

During the test, KCl solution was circulated across the top specimen boundary while DIW was circulated across the bottom boundary to create a concentration gradient. The use of the closed-system apparatus prohibits specimen volume change or osmotic counter-flow from occurring (see Malusis et al., 2001 for details). The concentrations of KCl source solutions (C_{ot}) ranged from 5 to 400 mM, to cover an equivalent range of average pore water concentrations of the specimen in the hydraulic conductivity test. Similar to previous studies, the circulation rate for the solutions was 22 mL/d, which has been considered reasonably

sufficient for assumption of constant concentration boundary conditions (Malusis et al., 2001).

The test started with first circulating DIW across both boundaries of the specimen to establish a baseline pressure difference (ΔP_o) . Then the diffusion and membrane efficiency measurements were initiated by circulating 5 mM KCl across the top boundary ($C_{ot} = 5 \text{ mM}$), while maintaining DIW circulation at the bottom boundary. If the specimen exhibits membrane behavior, a differential pressure (ΔP) will develop due to the applied concentration difference with chemico-osmotic counter-flow being restricted from occurring, based on the monitored pressures at the top and bottom boundaries, i.e., $\Delta P (=P_{top} - P_{bottom})$. Outflows were collected from both boundaries to monitor changes in EC and chloride concentration (C_{Cl}) with time. During the test, Cl⁻ diffuses from the top boundary (salt solution side) to the bottom boundary (DIW side), resulting in a decreased C_{Cl} along the top boundary ($C_t \leq C_{ot}$), and an increased C_{Cl} along the bottom boundary ($C_b >$ - $C_{\rm ob}$). Thus, the average boundary concentrations were calculated as:

$$C_{t_ave} = (C_{ot} + C_t)/2; C_{b_ave} = (C_{ob} + C_b)/2$$
 (12)

Steady-state diffusion and pressure conditions were achieved for each stage before increasing the C_{ot} to start the next concentration stage.

For each KCl stage, D^* for Cl⁻ was determined using the steady-state (time-lag) approach whereby the cumulative diffusive mass flux of Cl⁻ (Q_t ', mg/m²) from the bottom outflow was calculated based on concentration measurements and plotted as a function of cumulative elapsed time (t') for each concentration stage (Shackelford, 1991). The steady-state D^* can then be calculated by using a best-fit linear regression to the steady-state portion of the Q_t -vs-t curve (Shackelford and Lee, 2003), that is:

$$D^* = -\left(\frac{\Delta Q_t'}{\Delta t'}\right) \left(\frac{L}{nw_A \Delta C}\right) \tag{13}$$

where L is the specimen thickness, ΔC is the differential solute concentration across the specimen (i.e., C_{t_ave} - C_{b_ave}), and w_A , for this study, is the molecular weight of Cl⁻, i.e., 35.453 g/mol.

Table 2 Summary of the testing results from multi-stage hydraulic conductivity test.

Actual KCl Concentration in Permeant for Each Stage	Duration of Permeation for Each Concentration Stage		Volumetric Flow Ratio at End of Stage	•	Hydraulic Conductivity at End of Stage
C_{Cl} - (mM)	t (d)	PVF	$Q_{ m out}/Q_{ m in}$	$EC_{\text{out}}/EC_{\text{in}}$	$k \ (\times \ 10^{-11} \ \text{m/s})$
0	50	2.8	1.1	_	1.22
2.5	78	3.1	0.95	0.98	1.27
5.1	94	4.5	0.96	0.97	1.20
9.9	91	4.3	0.99	1.0	1.15
99	109	11	1.0	1.1	2.88
211	102	12	1.0	1.1	2.71

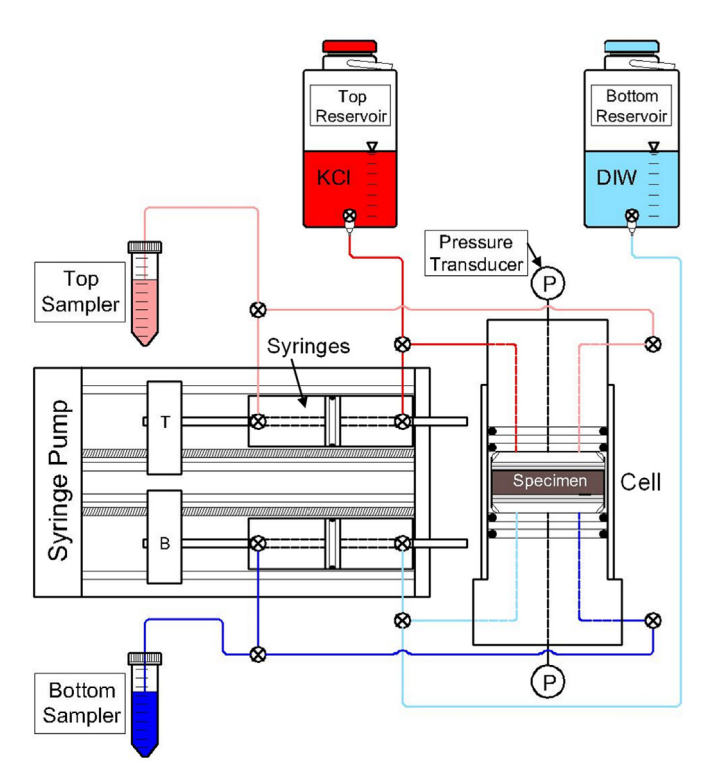


Fig. 1. Schematic of closed-system, through-diffusion testing apparatus used for measuring membrane behavior and diffusion through BPC-3.2 (similar apparatus design to Malusis et al., 2001).

Values of ω at steady-state for each KCl stage were calculated as follows (Malusis et al., 2001):

$$\omega = \Delta P_e / \Delta \pi = \Delta P_e / (vRT\Delta C) \tag{14}$$

where ΔP_e is the measured effective differential boundary pressure (= $\Delta P - \Delta P_o$), $\Delta \pi$ is the theoretical maximum ΔP_e corresponding to an ideal semipermeable membrane at a particular concentration difference (ΔC) across the specimen in accordance with the van't Hoff equation, v is the number of ions per molecule of the solute (e.g., 2 for KCl), R is the universal gas constant (8.314 J/mol·K), and T is the absolute temperature (293 K for room temperature).

3.4. Analyses of coupled solute transport example scenarios

To evaluate the impact of membrane behavior on the long-term barrier performance of the BPC-3.2 as a typical bottom liner in a landfill, analyses of 1-D steady-state coupled mass transport of chloride were conducted for scenarios of a GCL and a composite liner comprising a GCL and an attenuation layer (AL). Schematics of the two scenarios are shown in Fig. 2. The leachate head on top of the GCL was set to 300-mm (common maximum allowable height for leachate). The GCL was modelled as a 0.01-m-thick layer of bentonite. The thicknesses of the AL was 0.4 m.

The properties of the BPC-GCL were based on the measured k, D^* and ω from the multi-stage hydraulic conductivity test and the multi-stage through-diffusion/membrane

test in this study. The properties of the AL were selected to be the same as those used by Manassero et al. (2014) for a similar GCL/AL analysis, i.e., $k = 1.0 \times 10^{-7}$ m/s, $D^* =$ $9.0 \times 10^{-10} \,\mathrm{m}^2/\mathrm{s}$, $\omega = 0$, and n = 0.30. The applied boundary conditions were a constant source concentration at the upper boundary ($C_{ot} = 5, 10, 20, 50, 200, \text{ and } 400 \text{ mM}$) and a perfectly flushing condition at the bottom ($C_{ob} = 0$ mM). Calculation of the coupled solute mass flux through just the GCL (Fig. 2a) was performed in accordance with Equation (9). For the case of the GCL/AL (Fig. 2b), continuity of volumetric and mass fluxes was assumed at the interface between the GCL and the AL to solve the head difference concentration difference and across each (Manassero et al. (2014)). The reader is referred to Manassero et al. (2014) for additional examples of this approach for analysis of a GCL overlying an AL.

As indicated by the comparison of Equations (9) and (10), the existence of membrane behavior results in reduction of the total solute flux $(J'_j < J_j)$. This reduction can be expressed as the percentage reduction in solute flux (PRF) (e.g., Malusis et al., 2020):

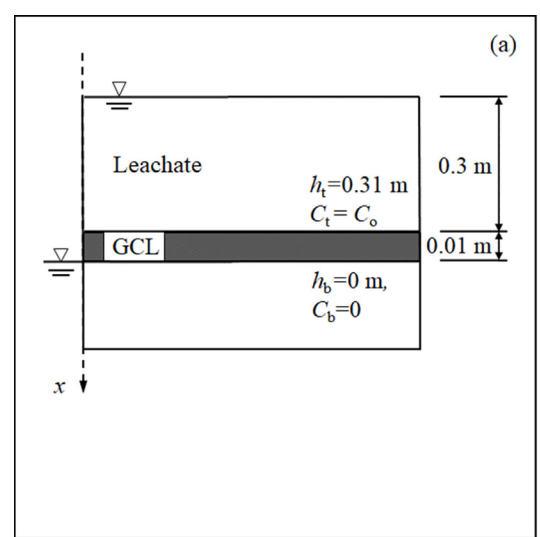
$$PRF = \frac{J_j(\omega = 0) - J'_j(\omega > 0)}{J_i(\omega = 0)} \times 100$$
 (15)

4. Experimental results

4.1. Hydraulic conductivity

The results of the multi-stage hydraulic conductivity test are summarized in Table 2. Six sequential test stages were performed at target permeant concentrations of 0 (DIW), 2.5, 5, 10, 100, and 200 mM. As the permeant concentration increased, the k of the BPC-3.2 specimen increased only by a factor of 2.2 (i.e., from 1.22×10^{-11} to 2.88×10^{-11} m/s). Due to the long duration of the test (i.e., 524 days), the concentration stages stepped directly from 10 mM to 100 mM, although in hindsight including an intermediate concentration (e.g., 50 mM) may have been beneficial. However, the increase in k from the 10 mM stage to the 100 mM stage was only by a factor of 1.5, which is minimal compared to increases in k reported for typical NaB-GCLs for solutions of similar concentration (e.g., > 1 order of magnitude).

The values of k for the BPC-3.2 were generally lower than that reported for NaB, but higher than that reported for BPC with higher polymer contents. For example, for 100 mM KCl, the k of the BPC-3.2 was 2.88×10^{-11} m/s, whereas that reported by Jo et al. (2001) for an NaB-GCL to the same solution was 4.0×10^{-11} m/s. For DIW, Tian et al. (2016a) reported the k for a BPC-GCL with a polymer mass content (X_p) of 12.7 % was 6.7×10^{-12} m/s, whereas that for the BPC-3.2 in this study was approximately-two times higher (1.22 \times 10⁻¹¹ m/s). The higher values of k measured in this study relative to that for BPC measured by, for example, Tian et al.



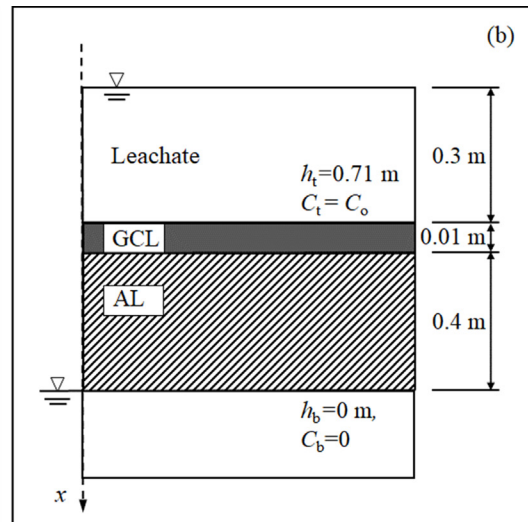


Fig. 2. Scenarios considered in the coupled transport analysis based on the experimental results: (a) scenario 1: geosynthetic clay liner (GCL); (b) scenario 2: GCL overlying an attenuation layer (AL).

(2016a) could be attributed to the lower X_p of the specimens (3.2 % < 12.7 %) and higher hydraulic gradient (300 in this study > 130 in Tian et al., 2016a) applied during the tests.

4.2. Effective diffusion coefficients

For the multi-stage diffusion/membrane test, the measured values of $C_{\rm Cl}$ of the outflows from the top and bottom specimen boundaries are plotted versus total elapsed time (t) in Fig. 3. During the baseline DIW stage (at test time < 0), $C_{\rm Cl}$ in the top and bottom outflows both decreased as the initial soluble ${\rm Cl}^-$ in the bentonite diffused out from the specimen. Once KCl solution was added to the top boundary (starting at t=0), $C_{\rm Cl}$ in both the top and bottom outflows rapidly increased within the first three to four circulations, indicating the quick replacement of the top circulating solution and the corresponding diffusion of ${\rm Cl}^-$ through the specimen. The $C_{\rm Cl}$ became constant for each stage as steady-state diffusion conditions were achieved.

To determine the D^* values of the BPC-3.2 in accordance with Equation (13), the Q_t -vs-t curves were plotted for each concentration stage (Fig. 4). The slopes of the linear regressions shown in Fig. 4 were used to calculate the D^* values listed in Table 3. As expected, the D^* for Cl⁻ increased with increasing solute concentration, with values of D^* increasing from 1.69 \times 10⁻¹⁰ to 4.43 \times 10⁻¹⁰ m²/s as C_{ave} increased from 2.58 to 227.1 mM. Increasing D^* with increasing C_{ave} in the pore water can be attributed to compression of the double layer around the montmorillonite particles and decreasing solute restriction, consistent with previous studies on membrane behavior and diffusion for NaB (e.g., Malusis and Shackelford, 2002b; Shackelford et al., 2016; Dominijanni et al., 2018) and BPC (Bohnhoff and Shackelford, 2015). The calculated τ_a value ranged from 0.08 to 0.22 (Table 3).

4.3. Membrane efficiency coefficients

Measured values of ΔP_e with time are shown in Fig. 5. Values of ω were calculated in accordance with Equation (14), using the ΔP_e data in Fig. 5 and outflow concentration data in Fig. 3. Values of ΔC used in Equation (14) were based on the average concentration difference across the specimen (i.e., $\Delta C = C_{t_ave} - C_{b_ave}$). The ω values decreased from 57.9 % to 0.4 % as C_{ave} increased from 2.5 to 200 mM, as summarized in Table 3. The decrease in ω with increasing pore concentration is consistent with expected reductions in solute restriction and results from prior experimental studies (e.g., Malusis and Shackelford, 2002a; Kang and Shackelford, 2011; Bohnhoff and Shackelford, 2013; Dominijanni et al., 2013; Meier et al., 2014; Tang et al., 2014; Sample-Lord and Shackelford, 2018).

Malusis and Shackelford (2002a) reported similar values of ω (0.16 to 0.58) for NaB for a similar KCl solution range (6.0 to 47 mM), but the specimen in their study had a lower porosity (n=0.86) than the specimen evaluated in this study (n=0.90). Shackelford et al. (2016) reported ω values for NaB GCL at similar n (n=0.79) that were closer to those measured for BPC-3.2 (e.g., for the 50 mM KCl stage: $\omega=0.043$ for NaB GCL versus $\omega=0.046$ for BPC-3.2 in this study). Given that membrane efficiency decreases as porosity increases, the ω results from this study reasonably compare with expected values based on the available literature.

4.4. Swell index

The swell index (*SI*) of BPC-3.2 was relatively high (i.e., 49.5 mL/2g) in DIW, and decreased from 37.0, 32.5, 18.0, 14.0, 8.0 to 5.7 mL/2g as KCl concentration increased from 10, 20, 50, 100, 200 to 400 mM. Most of the reduction in swelling occurred at dilute- to medium-level concentrations

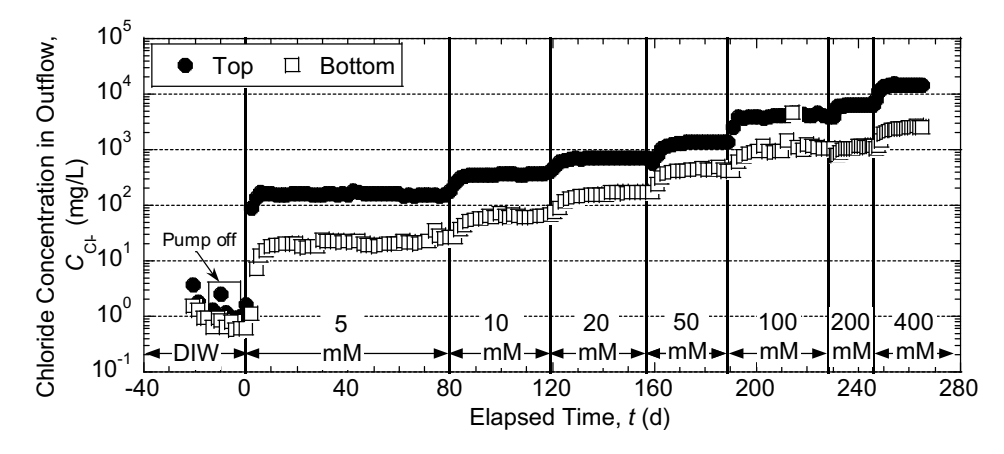
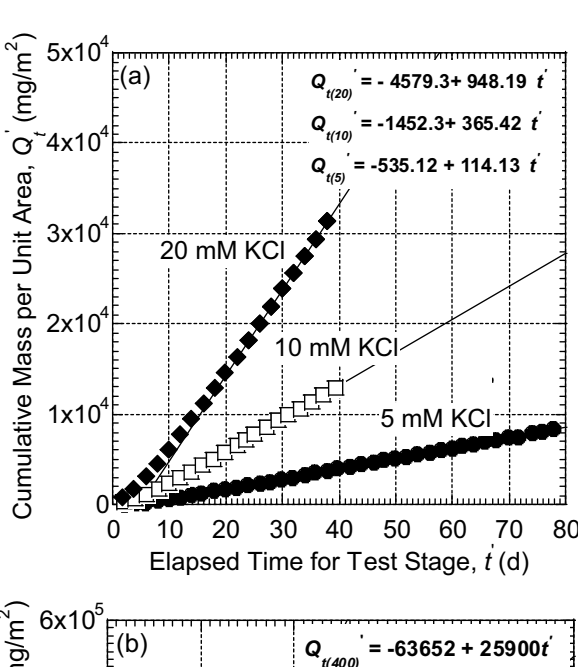


Fig. 3. Measured chloride concentrations (C_{Cl}) of the top and bottom outflows versus cumulative test time.



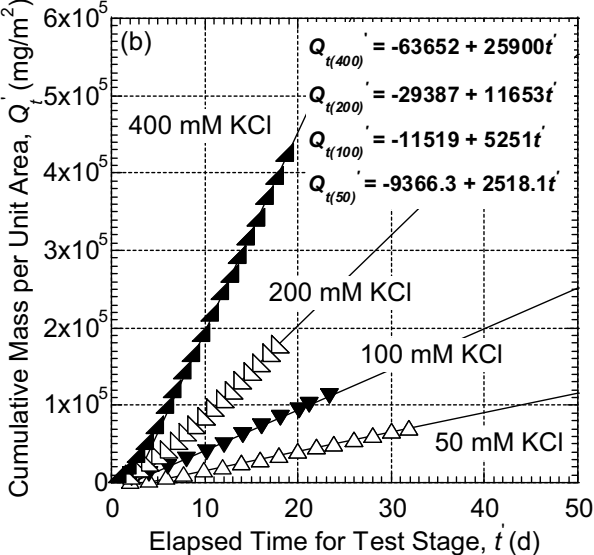


Fig. 4. Diffusion results for individual stages of multi-stage through-diffusion test: (a) 5, 10, and 20 mM KCl stages; (b) 50, 100, 200, and 400 mM KCl stages.

(0 to 50 mM), as shown Fig. 6(a). The values of SI of BPC-3.2 in DIW are similar to those reported by Tian et al. (2016a) for a BPC-GCL with X_p of 12.7 % (45 mL/2g).

To supplement the BPC-3.2 data, two series of parallel *SI* tests were conducted for just the NaB and sodium-polyacrylate-amended bentonite used to create the BPC-3.2 (Table 1), as shown in Fig. 6(a). As KCl concentration increased from 0 to 400 mM, *SI* of the NaB decreased from 32.0 to 5.3 mL/2g, whereas that of the sodium-polyacrylate-amended bentonite (noted just generally as "BPC" in the Fig. 6(a)) decreased from 71.0 to 12.5 mL/2g. The results are consistent with the range of 25.5 to 5 mL/2g reported for a similar NaB-GCL to KCl concentration ranging from 5 to 1000 mM (Jo et al., 2001), and the range of 46.5 to 10.5 mL/2g for the same BPC to KCl concentrations ranging from 20 to 1500 mM (Bohnhoff, 2012).

5. Analysis and discussion

5.1. Effect of polymer enhancement

Fig. 6(b-d) include a comparison of measured k, D^* , and ω as a function of average Cl⁻ concentration in the bentonite specimen for three different materials: (1) BPC-3.2 tested in this study ($X_p = 3.2$ %); (2) "BPC" tested by Scalia et al. (2014) ($X_p = 28.5$ %); and (3) GCL-grade NaB (without polymer) tested by Malusis and Shackelford (2002b). For measurement of k, all three studies used KCl solutions. As shown in Fig. 6(b), the k of the BPC-3.2 was lower than the k of the NaB without polymer, but higher than the k of the BPC with the higher polymer content.

For measurement of D^* and ω , all three studies used KCl solutions and the same type of closed-system apparatus, allowing for comparison of the results. The tests with most similar porosities were chosen for comparison of the diffusion and membrane behavior data in Fig. 6(c,d); i.e., n = 0.90 for the BPC-3.2 in this study, n = 0.92 for the BPC ($X_p = 28.5$ %) in Bohnhoff and Shackelford

Table 3
Summary of results from multi-stage diffusion and membrane behavior tests.

Test Stage So Concentration C_{ot} (mM)		Measured Effective Diffusion Coefficient, D^* (× 10^{-10} m ² /s)	Calculated $D_{se} (\times 10^{-10} \text{ m}^2/\text{s})$ $[=D^*/(1-\omega)]$	Effective Boundary Pressure Difference, ΔP_e (kPa)	Membrane Efficiency Coefficient, ω (-)	Apparent Tortuosity Factor, τ_a (-) $[=D^*/D_o]$
Target	Actual					
5	4.8	1.69	4.01	12.39	0.579	0.08
10	10.6	1.09	4.01	12.39	0.379	0.08
20	21.4	2.48	3.30	11.73	0.247	0.12
20	21.4	3.27	3.69	10.59	0.114	0.16
50	57.5	2.10	2.24	0.22	0.046	0.16
100	122	3.19	3.34	9.33	0.046	0.16
200	221	3.18	3.23	8.03	0.015	0.16
200	231	3.93	3.96	8.43	0.009	0.19
400	418					
		4.43	4.45	7.56	0.004	0.22

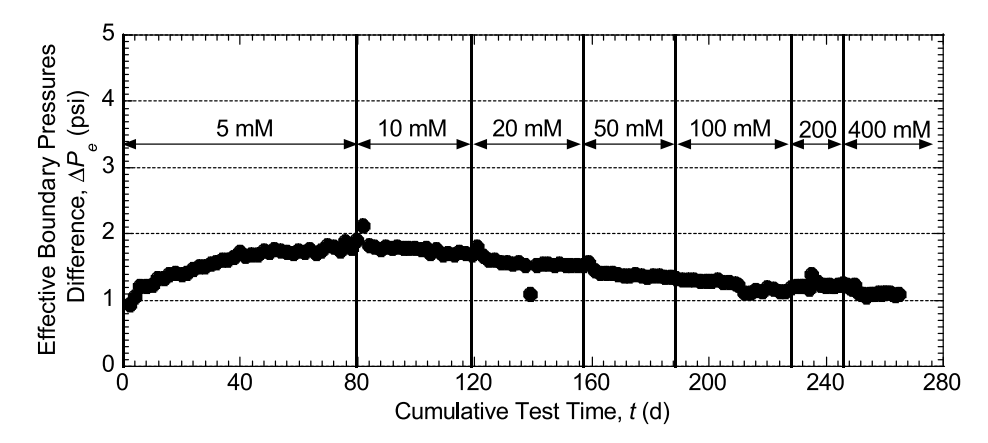


Fig. 5. Effective boundary pressure difference (ΔP_e) across the specimen during membrane behavior test.

(2015), and n = 0.86 for the NaB in Malusis and Shackelford (2002a,b). Note that the values of C_{ave} for the BPC-3.2 specimen from this study and Bohnhoff and Shackelford (2015) were calculated by averaging the top average concentration (C_{t_ave}) and bottom average concentration (C_{b_ave}). Values of C_{ave} for Malusis and Shackelford (2002a,b) were calculated by averaging the top source concentration (C_{ot}) and bottom source concentration (C_{ob}), based on the available data.

As shown in Fig. 6(c,d), all three materials exhibited increasing D^* and decreasing ω with increasing C_{ave} , consistent with the literature and expected trends due to double layer effects. For example, the D^* of NaB from Malusis and Shackelford (2002a,b) increased from 1.77×10^{-10} to 2.20×10^{-10} m²/s as C_{ave} increased from 10 to 23.5 mM (C_{ot} from 20 to 47 mM). The D^* for the BPC from Bohnhoff and Shackelford (2015) increased from 1.00×10^{-10} to 2.20×10^{-10} m²/s as C_{ave} increased from 2.35 to 27 mM. The ω of the NaB and BPC decreased from 2.35 to 2.35 mM and from 2.35 to 2.35 mM and from 2.4 mM to 2.35 mM, respectively.

For the BPC-3.2, the D^* values were slightly higher than the other materials at similar concentrations, and ω values were essentially similar to that for the NaB rather than BPC. Although the BPC with $X_p = 28.5 \%$ exhibited much higher membrane efficiency than the unamended NaB (Fig. 6d), surprisingly no corresponding improvement for diffusion (decrease in D^*) can be observed in Fig. 6c. Tong et al. (2021) measured diffusion coefficients for both unamended NaB and BPC for CaCl2 solutions using a dialysis-leaching test method (see Tong et al., 2019). The apparent diffusion coefficient (D_a) values for the BPC were lower than values for NaB for CaCl₂ source solutions up to 100 mM; however, at $C_o > 100$ mM, there was no discernible difference in the Da values for NaB and BPC (Tong et al., 2021). Although the literature has generally shown that increased polymer content in enhanced bentonites typically enhances hydraulic performance (Scalia et al., 2018), the impact of polymer amendment on diffusion and membrane behavior properties remains unclear and requires further study. Assessing the impact of polymer content on D^* and ω is likely complicated by differing

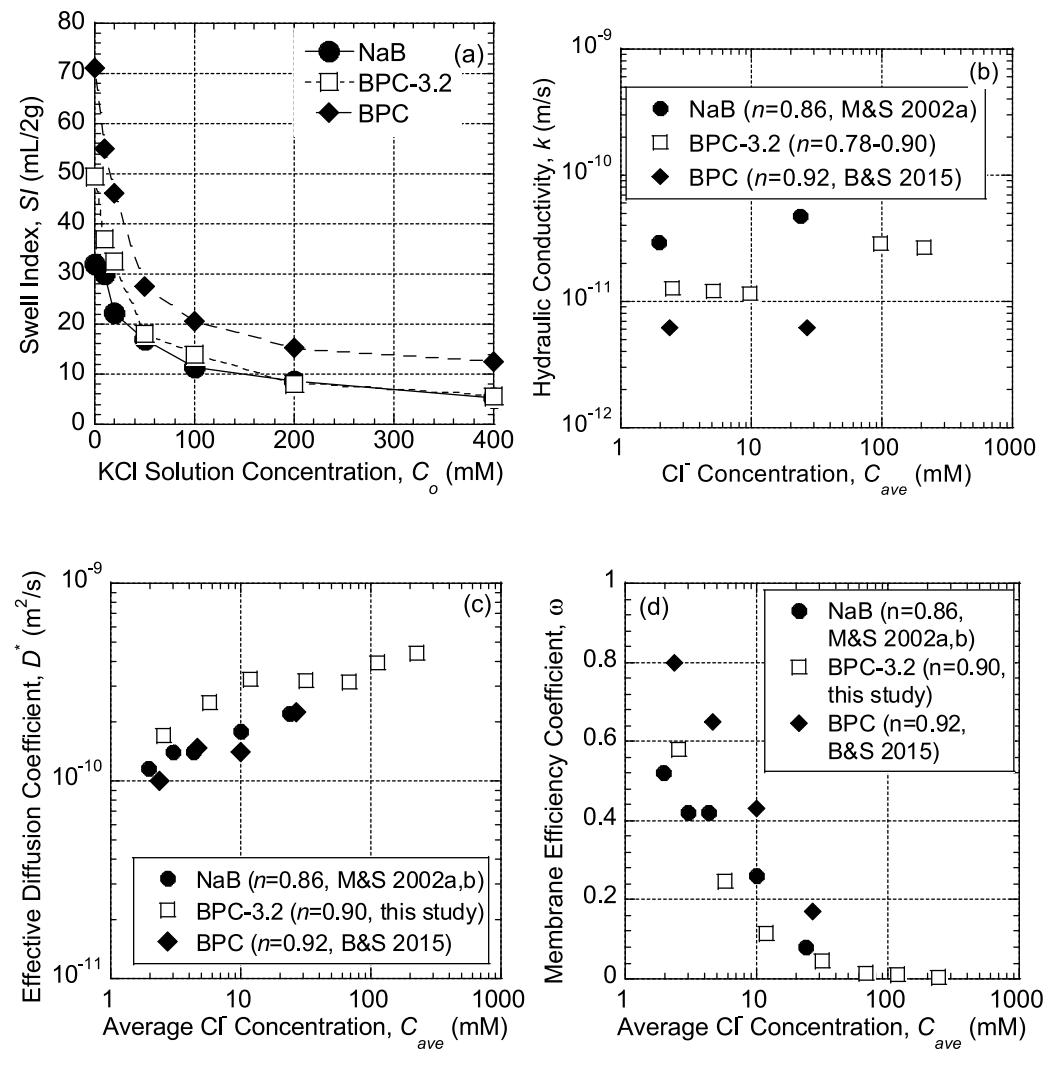


Fig. 6. (a) Swell index, (b) hydraulic conductivity, (c) effective diffusion coefficients, and (d) membrane efficiency coefficients as a function of average Cl⁻ concentration in the specimens. All tests were performed with KCl solutions. [M&S = NaB tested by Malusis and Shackelford 2002a,b; B&S = BPC with 28.5 % polymer content tested by Bohnhoff and Shackelford 2015].

properties of the polymer additives, structures/fabrics of the polymer-bentonite composite at micro- to macroscales and their changes with pore waster chemistry, as well as challenges associated with coupled membrane behavior and diffusion testing.

5.2. Coupled solute transport analysis examples

To evaluate the long-term performance of a barrier system containing an NaB- or BPC-GCL, coupled solute transport analyses were performed for the two scenarios in Fig. 2 and described previously. The same studies as shown in Fig. 6 were used to identify k, D^* , and ω values for the different GCL materials (i.e., NaB from Malusis and Shackelford (2002a,b), BPC with $X_p = 28.5$ % from Bohnhoff and Shackelford (2015), BPC with $X_p = 3.2$ % from this study). For scenario 1 (considering GCL only; Fig. 2a), the predicted impact of membrane behavior on the total solute mass flux through the three different GCLs

with their advective, diffusive and osmotic flux components are summarized in Fig. 7. In general, as C_{ot} increased from 5 to 400 mM, the magnitudes of J_{ss} , J_a , J_d and J_{π} for NaB, BPC-3.2 and BPC all increased by one to three orders of magnitude. Among the three transport components, the J_d values were consistently-one to two orders of magnitude greater than that of J_a , demonstrating the dominant role of diffusion for solute transport at low k. When membrane behavior was considered, i.e., when $\omega > 0$, values of J_{π} exceeded those of J_a (see the inset plots in Fig. 7a,c,e).

In Fig. 7b,d,f, the percentage reduction in solute flux (PRF) represents the reduction in total solute flux attributed to the existence of membrane behavior (see Equation (11)). The total height of each column represents the total percentage reduction in solute flux across the barrier, which is due to combined effects of three mechanisms associated with membrane behavior: hyperfiltration (reduction in advection), anion exclusion (reduction in diffusion), and chemico-osmotic counterflow (reduction due to counter-

flow towards the contaminant source). For most of the cases, reduction in diffusive flux due to anion exclusion is the greatest contributor to the total PRF and improved barrier performance. However, as the KCl source concentration increases the k of the bentonite and the concentration gradient both increase, leading to higher predicted

osmotic counter-fluxes that reduce the total solute flux through the barrier. Overall, neglecting the effects of membrane behavior for scenario 1 results in a 12 % to 60 % error in the predicted total solute mass flux through the BPC-3.2 GCL for a KCl concentration range of 57.5 mM down to 4.8 mM.

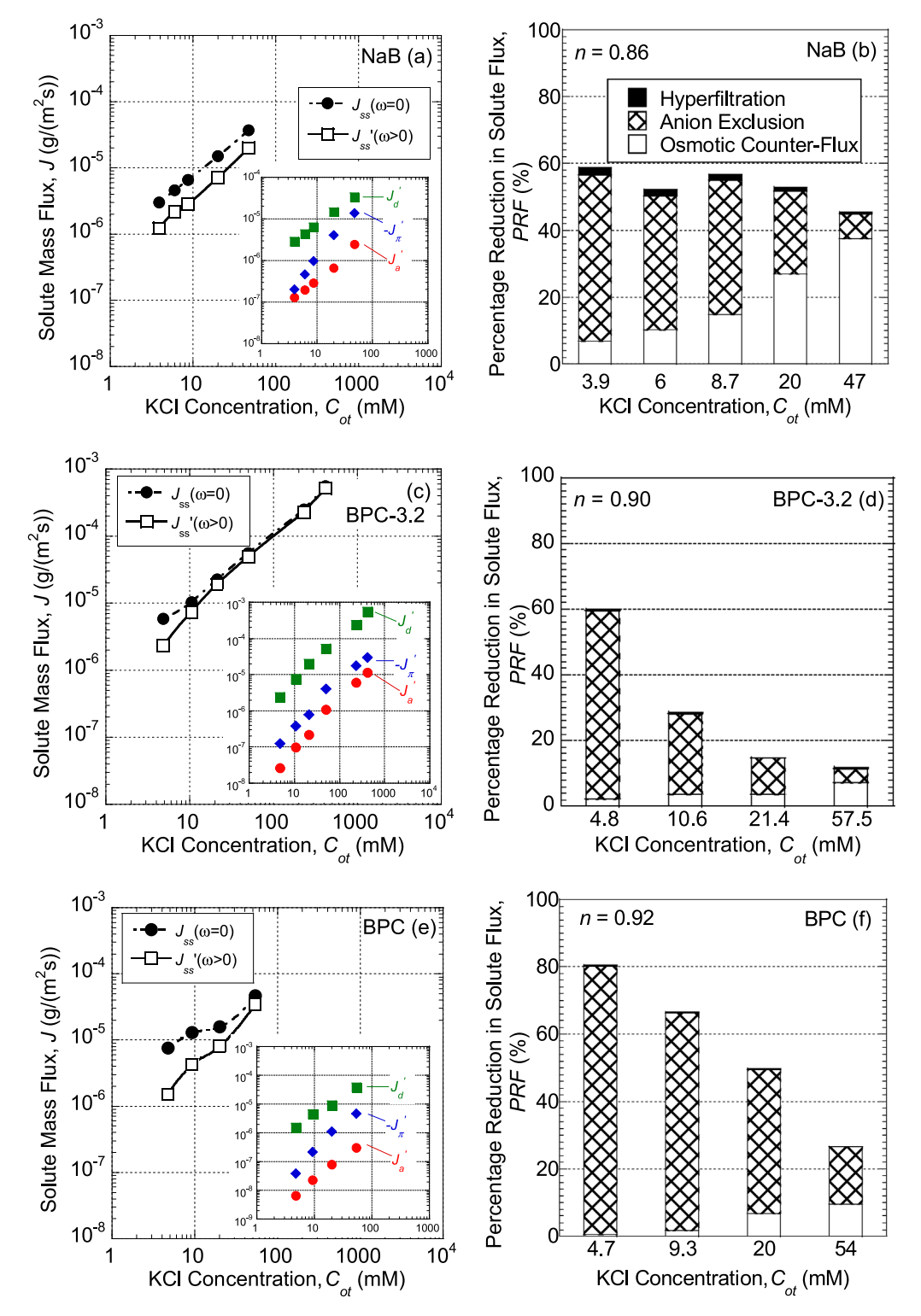
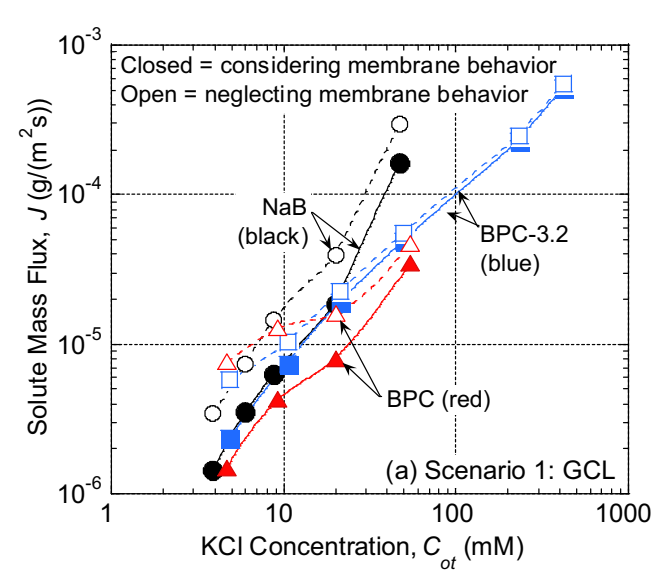


Fig. 7. Predicted solute mass fluxes through a GCL for (a) NaB (Malusis & Shackelford 2002a,b), (c) BPC-3.2, and (e) BPC with $X_p = 28.5$ % (Bohnhoff and Shackelford 2015), and the contribution to the percentage flux reduction by the three membrane behavior effects (b,d,f).

In scenario 2, an attenuation layer (AL) was added as described previously, and a similar analysis was carried out (see Section 3.4). A comparison of the results for the GCL (scenario 1) and GCL/AL (scenario 2) for all three bentonite types is provided in Fig. 8. The total solute mass flux when membrane behavior effects are considered is represented by the solid lines with closed symbols. In contrast, the dashed lines with open symbols represent the total solute mass flux when membrane behavior is ignored in the analysis. Over the range of concentrations considered and for both model scenarios, the total coupled solute flux through the barrier utilizing NaB was greater than that of the liners with BPC.

Consistent with the conclusions of a similar analysis that was performed by Manassero et al. (2014) for NaB-GCLs, the impact of considering chemico-osmotic counter-flow and hyperfiltration due to membrane behavior on the pre-



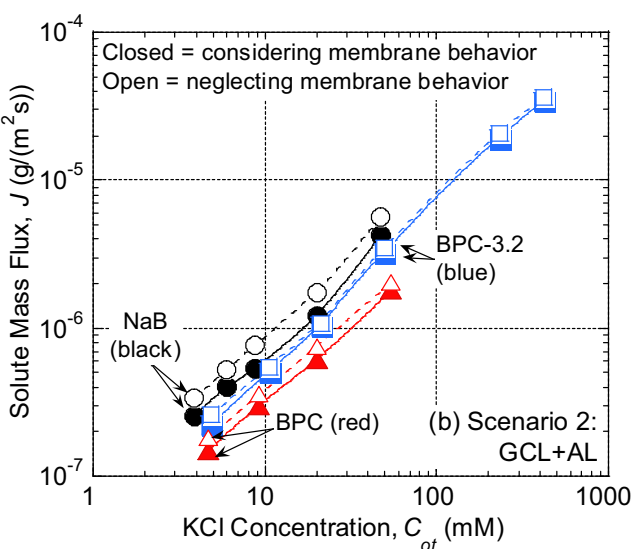


Fig. 8. Predicted solute mass flux through (a) GCL comprising either NaB, BPC-3.2, or BPC with $X_p=28.5\,\%$ (scenario 1), and (b) GCL plus attenuation layer (AL) (scenario 2).

dicted steady-state solute flux is more prominent for the scenario of a GCL alone, relative to the case of a GCL overlying an AL. As shown in Fig. 8a for the GCL only scenario, differences in predicted total solute flux when membrane behavior is accounted for versus when membrane behavior is ignored (i.e., the differences between the solid lines and the dash lines) are greater than differences observed for the GCL/AL scenario in Fig. 8b (i.e., the solid and dashed lines are closer in 8b). As expected, when an AL (which has been assumed to not exhibit any membrane behavior) is considered within the analysis of overall barrier performance, impacts due to membrane behavior exhibited by only the GCL layer diminish. For example, for BPC (red series) and a KCl source concentration of 10 mM, the total solute flux through a GCL (Scenario 1, Fig. 8a) increased from 4.3×10^{-6} g/m²s to 1.3×10^{-5} g/m²s when the membrane behavior was neglected. However, when the presence of an AL was also considered, the total solute flux for BPC at 10 mM only increased slightly when the membrane behavior was neglected (from $3.0 \times 10^{-7} \text{ g/m}^2\text{s}$ to $3.6 \times 10^{-7} \text{ g/m}^2\text{s}$, Fig. 8b).

6. Conclusions

Effective diffusion coefficients (D^*), membrane efficiency coefficients (ω), and hydraulic conductivity values (k) were measured for BPC with 3.2 % polymer content (BPC-3.2) for a wide range of KCl solutions (0 to 400 mM). Based on the multi-staged diffusion/membrane behavior test, values of D^* increased as C_{ave} of Cl^- increased, consistent with expectations based on double-layer and diffusion theories. Comparison of the diffusion results for BPC-3.2 to the experimental literature for unamended NaB and also BPC at higher polymer content (28 %) suggests that PAAS additives do not provide a notable enhancement in diffusion performance (i.e., lower D^*) relative to conventional NaB. However, traditional approaches to evaluate diffusion coefficients of clay barriers based on Fickian diffusion may not be as accurate for polymer-bentonite composite systems.

For membrane behavior of the BPC-3.2, values of ω ranged from 0.4 % to 58 %. As expected, ω decreased as C_{ave} of Cl⁻ increased. In the comparison of ω values with NaB and BPC in the literature for similar KCl concentration ranges, the ω values of the BPC-3.2 were more similar to that of unamended NaB than the BPC with higher (28 %) polymer content. The results suggest that improvements in membrane efficiency may not occur for BPC with low polymer content (e.g., < 4 %).

The results of the diffusion, membrane behavior, and hydraulic conductivity tests were combined in an analytical model to evaluate coupled solute transport through a GCL and a GCL/AL. The results confirmed that, for the given model conditions: (1) diffusion would dominate transport through a BPC-GCL and an NaB-GCL; (2) the existence of membrane behavior can play a significant role in the flux

of solutes across the barrier (e.g., up to 80 % reduction in mass flux); and (3) reductions in diffusive flux from anion exclusion is the greatest contributor to the improved containment performance due to membrane behavior. The results of the study demonstrate the importance of considering diffusion and membrane behavior in the assessment of coupled solute transport through bentonite barriers and the impacts of polymer enhancement on long-term performance.

Acknowledgement

Financial support for part of this study was provided by the U.S. National Science Foundation (NSF) under Award Number 1812550. The authors thank Dr. Michael Malusis of Bucknell University for contributing components of the testing equipment.

References

- Benson, C.H., Meer, S.R., 2009. Relative abundance of monovalent and divalent cations and the impact of desiccation on geosynthetic clay liners. J. Geotech. Geoenviron. Eng. 135 (3), 169–176.
- Bohnhoff, G.L., Shackelford, C.D., 2013. Improving membrane performance via bentonite polymer nanocomposite. Appl. Clay Sci. 86, 83–98.
- Bohnhoff, G.L., Shackelford, C.D., 2015. Salt diffusion through a bentonite-polymer composite. Clays Clay Miner. 63 (3), 145–162.
- Bohnhoff, G.L., Shackelford, C.D., Sample-Lord, K.M., 2014. Calcium-resistant membrane behavior of polymerized bentonite. J. Geotech. Geoenviron. Eng. 140 (3), 04013029.
- Bohnhoff, G.L., 2012. Membrane behavior, diffusion, and compatibility of a polymerized bentonite for containment barrier applications. Ph.D. dissertation, Colorado State University. Fort Collins, CO.
- Chen, J.-N., Salihoglu, H., Benson, C.H., Likos, W.J., Edil, T.B., 2019. Hydraulic conductivity of bentonite-polymer composite geosynthetic clay liners permeated with coal combustion product leachates. J. Geotech. Geoenviron. Eng. 145 (9), 04019038.
- Di Emidio, G., Mazzieri, F., Verastegui-Flores, R.D., Van Impe, W., Bezuijen, A., 2015. Polymer-treated bentonite clay for chemicalresistant geosynthetic clay liners. Geosynthetic International 22 (1), 125–137.
- Dominijanni, A., Manassero, M., Puma, S., 2013. Coupled chemical-hydraulic-mechanical behaviour of bentonites. Geotechnique 63 (3), 191–205.
- Dominijanni, A., Guarena, N., Manassero, M., 2018. Laboratory assessment of the semipermeable properties of a natural sodium bentonite. Can. Geotech. J. 55 (11), 1611–1631.
- Dutt, G., Low, P.F., 1962. Diffusion of alkali chloride in clay-water systems. Soil Sci. 93, 233–240.
- Fu, X.-L., Zhang, R., Reddy, K.R., Li, Y.C., Du, Y.J., 2021. Membrane behavior and diffusion properties of sand/SHMP-amended bentonite vertical cutoff wall backfill exposed to lead contamination. Eng. Geol. 284 106037.
- Gates, W.P., Bouazza, A., 2010. Bentonite transformations in strongly alkaline solutions. Geotext. Geomembr. 28 (2), 219–225.
- Gustitus, S.A., Nguyen, D., Chen, J.-N., Benson, C.H., 2021. Quantifying polymer loading in bentonite-polymer composites using loss on ignition and total carbon analyses. Geotech. Test. J. 44 (5), 20200007.
- Hornsey, W.P., Scheirs, J., Gates, W.P., Bouazza, A., 2010. The impact of mining solutions/liquors on geosynthetics. Geotext. Geomembr. 28 (2), 191–198.
- Jo, H.Y., Katsumi, T., Benson, C.H., Edil, T.B., 2001. Hydraulic conductivity and swelling of nonprehydrated GCLs permeated with

- single-species salt solutions. J. Geotech. Geoenviron. Eng. 127 (7), 557-567
- Kang, J.-B., Shackelford, C.D., 2011. Consolidation enhanced membrane behavior of a geosynthetic clay liner. Geotext. Geomembr. 29 (6), 544– 556.
- Katchalsky, A., Curran, P.F., 1965. Nonequilibrium Thermodynamics in Biophysics. Harvard University Press, Cambridge, MA.
- Kemper, W., Rollins, J., 1966. Osmotic efficiency coefficients across compacted clays. Soil Science Society of America, Proceedings 30 (5), 529–534
- Kemper, W., van Schaik, J., 1966. Diffusion of salts in clay-water systems. Soils Sci. Soc. Am. Proc. 30, 534–540.
- Kolstad, D.C., Benson, C.H., Edil, T.B., 2004. Hydraulic conductivity and swell of nonprehydrated geosynthetic clay liners permeated with multispecies inorganic solutions. J. Geotech. Geoenviron. Eng. 130 (12), 1236–1249.
- Lake, C.B., Rowe, R.K., 2000. Diffusion of sodium and chloride through geosynthetic clay liners. Geotext. Geomembr. 18, 101–131.
- Li, Q., Chen, J.-N., Benson, C.H., Peng, D., 2021a. Hydraulic conductivity of bentonite-polymer composite geosynthetic clay liners permeated with bauxite liquor. Geotext. Geomembr. 49 (2), 420–429.
- Li, D., Zainab, B., Tian, K., 2021b. Effect of effective stress on hydraulic conductivity of bentonite-polymer geosynthetic clay liners to coal combustion product leachates. Environ. Geotech., 1–12
- Malusis, M.A., Daniyarov, A.S., 2016. Membrane efficiency and diffusive tortuosity of a dense prehydrated geosynthetic clay liner. Geotext. Geomembr. 44 (5), 719–730.
- Malusis, M.A., Shackelford, C.D., Olsen, H.W., 2001. A laboratory apparatus to measure chemico-osmotic efficiency coefficients for clay soils. Geotech. Test. J. 24 (3), 229–242.
- Malusis, M.A., Scalia, J., Norris, A., Shackelford, C.D., 2020. Effect of chemico-osmosis on solute transport in clay barriers. Environ. Geotech. 7 (7), 447–456.
- Malusis, M.A., Shackelford, C.D., 2002a. Chemico-osmotic efficiency of a geosynthetic clay liner. J. Geotech. Geoenviron. Eng. 128 (2), 97–106.
- Malusis, M.A., Shackelford, C.D., 2002b. Coupling effects during steadystate solute diffusion through a semipermeable clay membrane. Environ. Sci. Technol. 36 (6), 1312–1319.
- Malusis, M.A., Shackelford, C.D., Maneval, J., 2012. Critical review of coupled flux formulations for clay membranes based on nonequilibrium thermodynamics. J. Contam. Hydrol. 138–139, 40–59.
- Malusis, M.A., Dominijanni, A., Scalia, J., Guarena, N., Sample-Lord, K.
 M., Bohnhoff, G.L., Shackelford, C.D., Manassero, M., 2021.
 Assessing the influence of chemico-osmosis on solute transport in bentonite membranes based on combined phenomenological and physical modeling. JGS Special Publ. 9 (2), 37–44.
- Manassero, M., Dominijanni, A., 2003. Modelling the osmosis effect on solute migration through porous media. Géotechnique 53 (5), 481–492.
- Manassero, M., Dominijanni, A., Musso, G., Puma, S., 2014. Coupled phenomena in contaminant transport. In: 7th International Congress on Environmental Geotechnics, vol. 1, pp. 144–169.
- Mazzieri, F., Di Emidio, G., Van Impe, P.O., 2010. Diffusion of calcium chloride in a modified bentonite: Impact on osmotic efficiency and hydraulic conductivity. Clays Clay Miner. 58 (3), 351–363.
- Meier, A.J., Sample-Lord, K.M., Castelbaum, D., Kallase, S., Moran, B., Ray, T., Shackelford, C.D., 2014. Persistence of semipermeable membrane behavior of a geosynthetic clay liner. In: 7th International Congress on Environmental Geotechnics, Nov. 10-14, 2014, Melbourne, Australia, pp. 496–503.
- Mitchell, J.K., 1993. Fundamentals of Soil Behaviour, 2nd edn. John Wiley & Sons, New York.
- Muzny, C.D., Butler, B.D., Hanley, H.J.M., Tsvetkov, F., Peiffer, D.G., 1996. Clay platelet dispersion in a polymer matrix. Mater. Lett. 28 (4–6), 379–384.
- Rowe, R.K., 2012. Short- and long-term leakage through composite liners. Can. Geotech. J. 49 (2), 141–169.

- Rowe, R.K., Caers, C.J., Barone, F., 1988. Laboratory determination of diffusion and distribution coefficients of contaminants using undisturbed clayer soil. Can. Geotech. J. 25 (1), 108–118.
- Rowe, R.K., Quigley, R.M., Brachman, R.W.I., Booker, J.R., 2004.

 Barrier Systems for Waste Disposal Facilities. Taylor & Francis,
 London.
- Sample-Lord, K.M., Shackelford, C.D., 2018. Membrane behavior of unsaturated sodium bentonite. J. Geotech. Geoenviron. Eng. 144 (1), 04017102.
- Scalia, J., Benson, C.H., Bohnhoff, G.L., Edil, T.B., Shackelford, C.D., 2014. Long-term hydraulic conductivity of a bentonite-polymer composite permeated with aggressive inorganic solutions. J. Geotech. Geoenviron. Eng. 140 (3), 04013025.
- Scalia, J., Bohnhoff, G.L., Shackelford, C.D., Benson, C.H., Sample-Lord, K.M., Malusis, M.A., Likos, W.J., 2018. Enhanced bentonites for containment of inorganic waste leachates by GCLs. Geosynthet. Int. 25 (4), 392–411.
- Shackelford, C.D., 1991. Laboratory diffusion testing for waste disposal A review. J. Contam. Hydrol. 7 (3), 177–217.
- Shackelford, C.D., 2014. The ISSMGE Kerry Rowe Lecture: The role of diffusion in environmental geotechnics. Can. Geotech. J. 51 (11), 1219– 1242.
- Shackelford, C.D., Lee, J.M., 2003. The destructive role of diffusion on clay membrane behavior. Clays Clay Miner. 51 (2), 187–197.
- Shackelford, C.D., Meier, A.J., Sample-Lord, K.M., 2016. Limiting membrane and diffusion behavior of a geosynthetic clay liner. Geotext. Geomembr. 44, 707–718.

- Shackelford, C.D., 2013. Membrane behavior of engineered clay barriers for geoenvironmental containment: state of the art. In: GeoCongress 2012, ASCE, Oakland, California, United States, pp. 3419–3428.
- Tang, Q., Katsumi, T., Inui, T., Li, Z., 2014. Membrane behavior of bentonite-amended compacted clay. Soils Found. 54 (3), 329–344.
- Tian, K., Benson, C.H., Likos, W.J., 2016a. Hydraulic conductivity of geosynthetic clay liners to low-level radioactive waste leachate. J. Geotech. Geoenviron. Eng. 138 (2), 04016037.
- Tian, K, Benson, C.H., 2015. Effect of low-level radioactive waste leachate on hydraulic conductivity of a geosynthetic clay liner. In: Geosynthetics 2015, IFAI, St. Paul, MN, pp. 236–244.
- Tian, K., Likos, W.J., Benson, C.H., 2016b. Pore-Scale imaging of polymer-modified bentonite in saline solutions. Geo-Chicago 2016. GSP 271, 468–477.
- Tian, K., Likos, W.J., Benson, C.H., 2019. Polymer elution and hydraulic conductivity of bentonite-polymer composite geosynthetic clay liners. J. Geotech. Geoenviron. Eng. 145 (10), 04019071.
- Tong, S., Sample-Lord, K.M., Bohnhoff, G.L., Balken, A.B., Ahmed, M., 2019. Dialysis method to measure diffusion in sodium and enhanced bentonites. Geo-Congress 2019. GSP 312, 203–211.
- Tong, S., Sample-Lord, K.M., Bohnhoff, G.L., 2021. Diffusion through sodium and polymer enhanced bentonites exposed to dilute and aggressive solutions. Can. Geotech. J. 58 (5), 603–618.
- Wireko, C., Abichou, T., Tian, K., Zainab, B., Zhang, Z., 2022. Effect of incineration ash leachates on the hydraulic conductivity of bentonitepolymer composite geosynthetic clay liners. Waste Manage. 139, 25– 38.